ELSEVIER

Thermochimica Acta 342 (1999) 115–137

thermochimica acta

www.elsevier.com/locate/tca

Physical aging in poly(ethylene oxide)/*atactic*-poly(methyl methacrylate) blends

Juliette Vernel[a], Rodney W. Rychwalski[a,*], Vladimir Pelíšek[b,1], Petr Sáha[b], Marcus Schmidt[c], Frans H.J. Maurer[c,2]

[a]*Department of Polymeric Materials, Chalmers University of Technology, Göteborg, Sweden*
[b]*Faculty of Technology Zlín, Technical University Brno, Czech Republic*
[c]*Department of Polymer Technology, Chalmers University of Technology, Göteborg, Sweden*

Received 7 July 1999; accepted 12 August 1999

Abstract

Physical aging in poly(ethylene oxide)(PEO)/*atactic*-poly(methyl methacrylate) (*a*-PMMA) blends with a low content of PEO is discussed. Behaviour in the T_g-region is analysed. Different compositions are prepared by mixing in the melt, and were compared at the same temperature distance to mid-point enthalpic T_g. Macrolevel properties (enthalpy and external volume) are discussed in terms of the Tool–Narayanaswamy–Moynihan (TNM) model. In particular, the non-linearity x parameter (determined using the peak shift method), the apparent activation enthalpy Δh^*, and the combination $\theta \cdot (1-x)$, where $\theta = \Delta h^*/R \cdot T_g^2$, are used to discuss overall segmental co-operativity and relaxation in the blends. Based on aging in viscoelastic properties (aging rate), structural mobility is discussed. From obtained results, an increase of co-operativity, and decrease of both, relaxation rate and change of structural mobility, with the increasing content of PEO in the blend, is concluded for temperatures between the dilatometric and enthalpic T_g. Agreement with data from studies at the microlevel by other authors, where an onsetting with time phase separation in PEO/PMMA has been postulated, is found.

Keywords: Relaxation; Physical aging; Co-operativity; PEO/PMMA

1. Introduction

Polymer blends offer an attractive cost–performance alternative to unblended polymers. Evolution of physical properties originating from non-equilibrium in the glassy state, referred to in the literature as physical aging [1], can take place in polymer blends. Physical aging can be studied on the macro- and microlevel, and macrolevel measurement methods are well established. Generally, the advantage of any physical aging analysis is that it necessarily uses equilibrium as the starting point, and thus properties following the same thermal history are strictly comparable.

Several reports dealing with poly(ethylene oxide)-(PEO)/poly(methyl methacrylate)(PMMA) blends have been published in the literature since the 80s.

*Corresponding author. Tel.: +46-31-7721315; fax: +46-31-7721313

E-mail address: rodney@polymm.chalmers.se (R.W. Rychwalski)

[1]Visiting Research Student in the Department of Polymeric Materials, Chalmers University of Technology.

[2]Present address: Department of Polymer Science and Engineering, Center for Chemistry and Chemical Engineering, Lund University, Lund, Sweden.

0040-6031/99/$ – see front matter
PII: S0040-6031(99)00291-9

We can quote the works of Li and Hsu [2], Ramana Rao et al. [3], Russel et al. [4], Cimmino et al. [5], Pedemonte et al. [6], and Shimada and Isogai [7], as examples. Recently the blend has been investigated at the free volume level by means of the positron annihilation lifetime spectroscopy (PALS) [8–10], and the solid-state nuclear magnetic resonance (NMR) technique [11,12]. Also recently, an attempt was made to investigate the influence of physical aging in the blend at the chromophore level (∼5 nm) by means of the non-linear optical technique of second harmonic generation (SHG) [13].

In this paper we use macrolevel techniques. Differential scanning calorimetry (DSC), mercury-in-glass dilatometry and mechanical analyses are employed to obtain physical aging data. The only physical aging data for PEO/*a*-PMMA known to us have been reported by Chang [14], and more recently by Chang et al. [15], for solution mixed blends. Physical aging data for *atactic* PMMA are frequently available in the literature, for example in the works of Hutchinson and Bucknall [16], Greiner and Schwarzl [17], Tribone et al. [18] and Hutchinson [19].

It is commonly accepted that the PEO/PMMA blend is completely miscible in the melt but there are conflicting views regarding the level of mixing in the solid state. The single glass transition temperature observed for the blend is usually treated as a manifestation of complete miscibility. It is well known that glass transition temperature is related to the structural level of about 50 monomer units. Miscibility in the PEO/*a*-PMMA blend is discussed in papers by Wästlund and Maurer [9] and Schantz [12]. There are further interesting points related to miscibility. Recently, Sato et al. [20] reported a rather unusual for polymer blends upper critical solution temperature (UCST)-type miscibility, and decomposition in the solid state for a PEO blend containing poly(methyl methacrylate-stat-styrene) copolymer. Although this is not the same blend as studied in this paper, some similarities can be found. Also, Wästlund et al. [10] have confirmed spinodal decomposition onsetting with time, prior to crystallization, below UCST at approximately 70°C in a PEO/*a*-PMMA blend with 38 vol% PEO. The PEO/*atactic*-PMMA blend involves dissimilar polymers with much different glass transition temperatures (by about 150°C). It has been reported in the literature that dissimilarity in T_g is a source of concentration fluctuation causing broadening of the T_g-region [21]. Inhomogeneity in density changing during physical aging in a non-monotonic manner has been recently reported even for unblended PMMA [22].

In this paper we will analyse the influence of composition on relaxation behaviour and segmental co-operativity in order to better understand the blend. In particular, the behaviour of the blend in the T_g-region will be focused on. Results may be interesting to compare with time-dependent non-linear optical behaviour of the blend, and also towards the vexed case of miscibility.

2. Theory

We use the fractional exponential formulation known as the Kohlrausch–Williams–Watts function [23]:

$$\phi(t) = \exp\left[-\left(\int_0^t \frac{\mathrm{d}t'}{\tau}\right)^{\beta}\right]. \tag{1}$$

The convolution integral in Eq. (1) represents the so-called reduced time. β is the non-exponentiality parameter ($0 < \beta \leq 1$) inversely proportional to the width of distribution of relaxation times. When τ is constant the above equation simplifies to the convenient and well familiar form given below:

$$\phi(t_a) = \exp\left[-\left(\frac{t}{\tau}\right)^{\beta}\right], \tag{2}$$

where t is time, and τ is the characteristic relaxation time.

A common expression to describe the dependence of t in glassy relaxation is known as the TNM equation, and is associated with the names of Tool [24], Moynihan et al. [25], and Narayanaswamy [26]:

$$\tau = \tau_0 \cdot \exp\left[\frac{x \cdot \Delta h^*}{R \cdot T_a} + \frac{(1-x) \cdot \Delta h^*}{R \cdot T_f}\right]. \tag{3}$$

In Eq. (3), R denotes the ideal gas constant, T_a denotes the aging temperature, T_f denotes the fictive temperature (in our work equivalent to the limiting fictive temperature, T_f', in Moynihan et al. [25]), t_0 denotes the pre-exponential factor which in equilibrium at an infinitely high temperature ($T_a = T_f = \infty$) is equal to

τ, and Δh^* denotes the apparent activation energy found in the usual way by assuming the Arrhenius formalism. The Narayanaswamy non-linearity parameter x (non-linearity is introduced when $x < 1$) defines the relative contributions of temperature (T_a) and structure (T_f) to the calculated characteristic relaxation time, τ (see Eq. (3)). More detailed descriptions can be found in review articles by Hodge [27] and Hutchinson [28].

Relaxed enthalpy ΔH increases on aging. The equilibrium value is denoted ΔH_∞. ΔH is often normalised as follows:

$$\phi(t_a) = 1 - \frac{\Delta H(t_a)}{\Delta H_\infty}. \quad (4)$$

Above function describes the kinetics of relaxed enthalpy and changes from 1 (unaged material) to 0 when the material attains equilibrium. It is generally accepted for physical aging that ϕ is described by Eq. (1) with τ given by Eq. (3). It is interesting to note that Eq. (2) has been employed to describe physical aging. In CF (Cowie–Ferguson) modelling of relaxed enthalpy, all parameters in Eqs. (2) and (4) are adjusted by using curve-fitting algorithm [29,30]. The TNM model has been remarkably successful in predicting enthalpy relaxation and thermograms at constant heating speed. Non-linearity in physical aging (of which behaviour the asymmetry of contraction and expansion evolutions following temperature down-, and up-jumps is a spectacular case) has been widely interpreted in terms of the TNM equation [31]. In fact, Kovacs et al. [32] have shown that several other proposed relations for τ can all be written in the form of Eq. (3). Although the model is phenomenological it uses parameters that may be regarded as characterizing the structure. We use this in the paper. Details are explained further ahead in Section 5.

3. Experimental

3.1. Material

Blends of *a*-PMMA (6N, Röhm, density $\rho = 1.19$ g/cm^3, molecular mass $M_w = 90$ kg/mol, mid-point enthalpic $T_g = 95°C$) with 0, 6, 10 and 14 vol% of PEO (Scientific Polymer Products, $\rho = 1.21$ g/cm^3, $M_w = 200$ kg/mol, mid-point enthalpic $T_g = -65°C$) were prepared by melt mixing (further in the text referred to as 00/100, 06/94, 10/90 and 14/86 PEO/*a*-PMMA). It should be noted that PMMA used in this work contains 6 mol% methyl acrylate (random placement) as determined by ^{13}C NMR [11,12]. All materials including 00/100 PEO/PMMA were processed in a Brabender melt mixer. Polymers were dried for 12 h and were mixed at 190°C for 15 min at 7 rev/min. Plaques were compression moulded (15 min, 190°C, 500 kPa). In the following testing it was observed that no changes of measured properties took place after several excursions to 190°C, and thus it was assumed that there was no degradation. Samples were annealed in a poly(oxymethylene) (POM) die (12 h, $T_g + 10°C$) for the purpose of degassing and stress removal, and were placed in a desiccator until further tested. When subsequently measured they remained in a dry environment.

3.2. Apparatus and sample

3.2.1. DSC

Perkin-Elmer DSC 7 calorimeter with high purity nitrogen as purge gas was used for enthalpic measurements. A dual-stage closed-loop circulating heat exchanger (Intracooler 2 from Perkin-Elmer) was used for cooling. Calorimeter was calibrated using an indium standard. Typically a 7 mg sample was placed in a standard aluminum pan. To ensure good contact, the pan was heated to 180°C and closed while the polymer was still soft. Measurements for each blend were conducted in a continuous series of cool–heat cycles or isothermally, without removing the sample from the instrument. In-instrument aging, generally, has the drawback that daily adjustment cannot be made, when necessary, to the baseline. This aging option was accepted after observing that thermograms well superpose (as shown in Fig. 1), meaning that the daily adjustment to the baseline was not necessary. On the other hand, keeping the sample in the instrument, as it was also in the case of dilatometric and mechanical measurements in this study, eliminated the possibility of accidental environmental influences, and gave reproducible results. Higher aging temperatures were used to shorten the occupation of the instrument.

It is well known that T_g measurements by DSC have an error of about 1°C and thus we report values with two significant figures. Enthalpy measurements had an estimated accuracy of $\pm$ 0.1 J/g. Mid-point T_g was

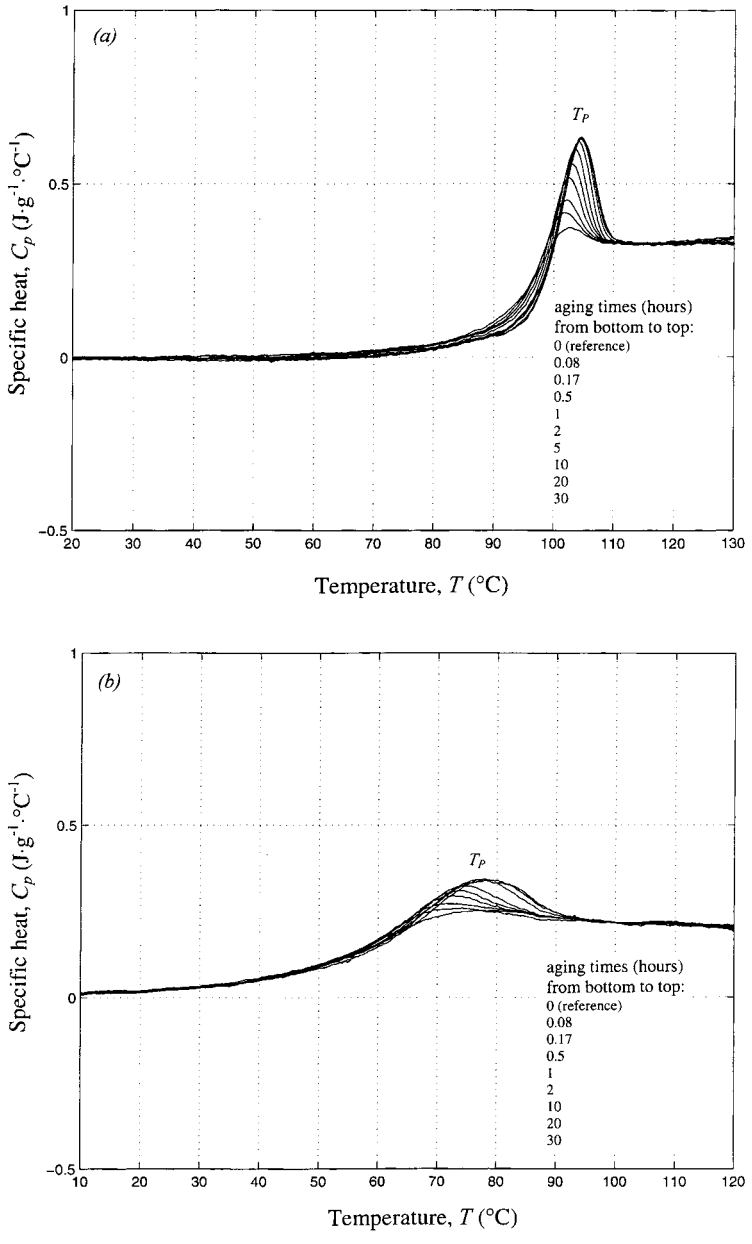

Fig. 1. DSC thermograms measured during aging at temperatures $T_a = T_{g,enth.} - 5°C$ equally positioned relative to respective $T_{g,enth.}$ for: (a) 00/100 PEO/*a*-PMMA, and (b) 14/86 PEO/*a*-PMMA. Aging times are given in the inset table. T_p is the peak temperature, that is the temperature at which the specific heat, C_p, is maximum.

calculated using instrument software. On the other hand, special software based on the work by Moynihan et al. [25] was developed by us to calculate the fictive temperature (description is given further ahead in Section 4.1.3).

3.2.2. Mercury-in-glass dilatometry

Dilatometers were constructed following ASTM Standard D864-52. Filling procedure is described elsewhere [33]. Vacuum of the order of 10^{-5} bar for 72 h at 20°C was used for air/gas evacuation.

The accuracy of volume measurements was about 1×10^{-5} cm^3/cm^3. This was assessed from the smallest measurable volume change ($=2.8\times10^{-5}$ cm^3) and the typical sample size (about 2.7 cm^3). A thermostatically controlled bath (Grant W14-ZD) filled with silicon fluid, equipped with a digital temperature controller was used. Temperature fluctuations of the bath were ±0.004°C (given by the manufacturer). Bath was placed in a temperature controlled environment (±1°C).

3.2.3. Mechanical analysis

Torsional mode dynamic mechanical analysis (DMA) and stress relaxation measurements were carried out by using Rheometric Scientific RDA2 mechanical spectrometer equipped with a special fixture for solids (torsional rectangular). Samples, for example 12.2 × 5.98 × 1.76 mm^3, were cut from annealed bars using a low speed diamond saw, and were finished with fine sand-paper. Direct mounting of samples in the instrument introduced undesirable effects, as described in [33], and therefore metal clamps were bonded to sample ends before mounting. Selected frequencies of 0.1, 0.314, 1, 3.14 and 10 Hz were used (DMA). The strain level did not exceed 0.1% (DMA) and 0.05% (stress relaxation), tested to be within the linear range. Measurements were made over a number of cycles (DMA) following the manufacturer's programmed routines, at the five selected frequencies, at approximately equal intervals of logarithmic time following thermal equilibration after the quench. Commonly accepted proportion of testing time to aging time <0.1 was observed. The same sample was used throughout each series, and the time intervals between measurements were always sufficient to allow full recovery. The dimensions of all specimens were checked after each series of aging experiments to verify that dimensional stability had been maintained, essential for accurate and reproducible measurements. Further details can be found in [33]. Both types of experiments, dynamic mechanical and stress relaxation ones, were conveniently controlled and data were acquired using instrument RHIOS software. Temperature programmes are described in the following section.

4. Results and analysis

4.1. Enthalpic results

4.1.1. Intrinsic cycles

The first set of experiments is referred to as intrinsic cycles. Samples were heated at a rate of +10°C/min through their glass transition temperature, following cooling from equilibrium at a temperature well above glass transition, at rates varied between –0.25 and –50°C/min. Apparent activation enthalpy, Δh^*, was calculated from the cooling rate dependence of the fictive temperature, in the well known way. An example (for PMMA) is shown in Fig. 3. Results are given in Table 1. Also in Table 1, glass transition temperature of the blends following a cooling rate of –7.5°C/min is given, where it is denoted $T_{g,enth.}$. This cooling rate was selected as close to the ones available in dilatometric and mechanical experiments (described further ahead). $T_{g,enth.}$ was measured by mid-point construction given by the instrument. It is believed that mid-point T_g is more reproducible than other calorimetric definitions of T_g [34,35].

4.1.2. Isothermal enthalpy relaxation

Throughout this paper, we compare blends at the same negative temperature distance to $T_{g,enth.}$. $T_{g,enth.}$

Table 1
Enthalpic results (case I)

Material	00/100	06/94	10/90	14/86
$T_{g,enth.}$ (°C)	95	82	76	61
ΔC_p(J/g·°C)	0.310	0.287	0.264	0.229
ln τ_0 (s)	–400.9 ± 36	–288.3 ± 25	–334.3 ± 29	–220.9 ± 18
Δh^* (kJ/mol)	1240 ± 124	864 ± 86	983 ± 98	626 ± 63
x	0.40 ± 0.06	0.20 ± 0.06	0.24 ± 0.06	
$\theta\cdot(1-x)$ (K^{-1})	0.66	0.66	0.74	
$\Delta H_{\infty,extra}$ (J/g)	1.55 ± 0.16	1.44 ± 0.14	1.32 ± 0.13	1.15 ± 0.12

was determined by means of DSC with an approximation typical for this technique. Thus the actual temperature distance was similarly approximate. In fact, the accuracy of $T_{g,enth.}$ worsened with the increasing PEO content. For this reason the 14/86 blend where the scatter in $T_{g,enth.}$ was not less than $\pm 3^{\circ}C$ could not be included in the analysis. The DSC technique of measuring T_g yielded relatively high T_g compared to other techniques. Thus, at a selected negative temperature distance to T_g the timescale for equilibrium was relatively short. Shorter timescales were desirable for practical reasons. Also, temperature down-jumps necessarily from equilibrium in the liquid to a temperature below T_g, in the case of $T_{g,enth.}$ involved a smaller temperature step which was preferred. By selecting a small distance to the glass transition temperature it was possible to realise aging both, below and slightly above enthalpic T_g, by varying the cooling rate. This will be explained.

Two temperature programmes denoted case I and II were used. For case I, a constant negative temperature distance to $T_{g,enth.}$ of $5^{\circ}C$ was used. Samples were annealed at $T_{g,enth.} + 50^{\circ}C$ for 5 min in order to erase any previous thermal history; cooled down to the aging temperature, T_a, at a cooling rate $q_0 = -7.5^{\circ}C/min$; aged at T_a for time t_a, and then cooled down to $T_{g,enth.} - 100^{\circ}C$ at a cooling rate $q_0 = -7.5^{\circ}C/min$. Next, the sample was scanned from $T_{g,enth.} - 100^{\circ}C$ to $T_{g,enth.} + 50^{\circ}C$ at a heating rate of $+10^{\circ}C/min$ and the aged thermogram was recorded. A second temperature scan was obtained by repeating the same sequence but with $t_a = 0$ (the unaged, reference scan) which was used together with the aged thermogram to calculate the relaxed enthalpy. In case II, a small temperature distance of $-2^{\circ}C$ was used. Samples were annealed at $T_{g,enth.} + 15^{\circ}C$ for 1 h; cooled down to the aging temperature, T_a, at a low cooling rate of $q_0 = -0.5^{\circ}C/min$; aged at T_a for a period of time t_a, and then cooled down to $T_{g,enth.} - 100^{\circ}C$ at a cooling rate of $q_0 = -40^{\circ}C/min$. Next, the sample was scanned from $T_{g,enth.} - 100^{\circ}C$ to $T_{g,enth.} + 50^{\circ}C$ at a heating rate of $10^{\circ}C/min$. Similarly as before, a reference scan was obtained.

The excess enthalpy lost on aging at temperature T_a during time t_a is commonly referred to as relaxed enthalpy, $\Delta H(t_a, T_a)$, and is given by the following integral:

$$\Delta H(t_a, T_a) = \int_{T_A}^{T_B} (C_{p,aged}(T) - C_{p,unaged}(T))\, dT, \quad (5)$$

where T_A is a temperature well below the glass transition, and T_B is a temperature above the glass transition at which the heat capacity is equal to the equilibrium liquid value at constant pressure (C_{pl}). As an example, a sequence of thermograms evolving on aging for the 00/100 and 14/86 PEO/*a*-PMMA blends at $T_a = T_{g,enth.} - 5^{\circ}C$ is shown in Fig. 1 (aging times are indicated in the inset table).The evolution of ΔH at $T_a = T_{g,enth.} - 5^{\circ}C$ (for three blends) and at $T_{g,enth.} - 2^{\circ}C$ (for two blends) is shown in Fig. 2. ΔH data for PMMA can be compared with results of other authors published in the literature. For example, Pérez et al. [36] measured ΔH slightly in excess of 0.5 J/g after an aging time of about 13 h at a temperature of $93^{\circ}C$ ($29^{\circ}C$ below T_g, given by the authors) compared to our result of about 0.8 J/g after a similar time at a lower temperature of $90^{\circ}C$. Cowie and Ferguson [37] measured ΔH close to 0.9 J/g after aging for a similar time at a temperature of $114.5^{\circ}C$, for a PMMA having a T_g (calorimetrically) of $122^{\circ}C$.

4.1.3. Calculation of the TNM parameters

Calorimetric data are used to calculate the fictive temperature T_f, the apparent activation enthalpy Δh^*, the nonlinearity parameter x, and also $\theta \cdot (1-x)$, where $\theta = \Delta h^* / R \cdot T_g^2$ is the reduced effective activation energy first introduced in the KAHR (Kovacs–Aklonis–Hutchinson–Ramos) model [38]. Parameter $\theta \cdot (1-x)$ was recently derived from the TNM equation by Málek and Montserrat [39]. x, Δh^* and $\theta \cdot (1-x)$ results are shown in Table 1, and are discussed in Section 5.3, where also discuss the remaining TNM parameters are discussed.

As mentioned before, we preferred to use the equal area construction by Moynihan et al. [25] to obtain T_f. We note that it is important to proceed from well superposing thermograms with well overlapping asymptotes. Same limiting temperatures sufficiently away from the transition region were used in this work. The fictive temperature was calculated by using a special software developed by us in the MATLAB environment. Next, the apparent activation enthalpy, Δh^*, was calculated. In Fig. 3, a plot of

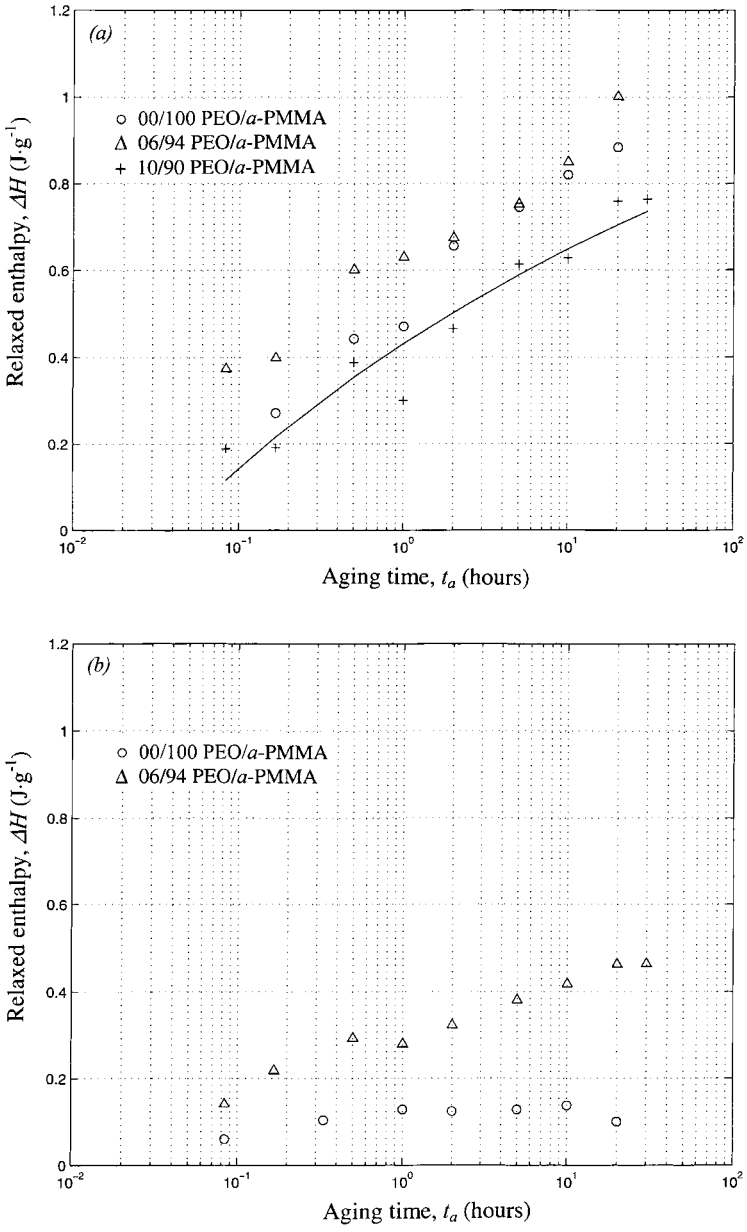

Fig. 2. Relaxed enthalpy vs. time for blends aged at: (a) $T_a = T_{g,enth.} - 5°C$, and (b) $T_a = T_{g,enth.} - 2°C$. Solid line is a trend/regression line for the 10/90 PEO/*a*-PMMA blend.

ln (q_1/q_0) vs. $1/T_f$ is shown for the 00/100 blend, as an example. Δh^* is calculated in an "apparent" way, that is by assuming Arrhenius formalism and interpolating experimental data with a straight line. Parameter x was calculated by using the peak shift method developed by Hutchinson and Ruddy [40]. As an example, a plot of peak temperature, T_p, vs. relaxed enthalpy, ΔH, for the10/90 blend is shown in Fig. 4. T_p is the peak temperature (the temperature at which C_p is maximum, see Fig. 1). Slope of this plot gives access to

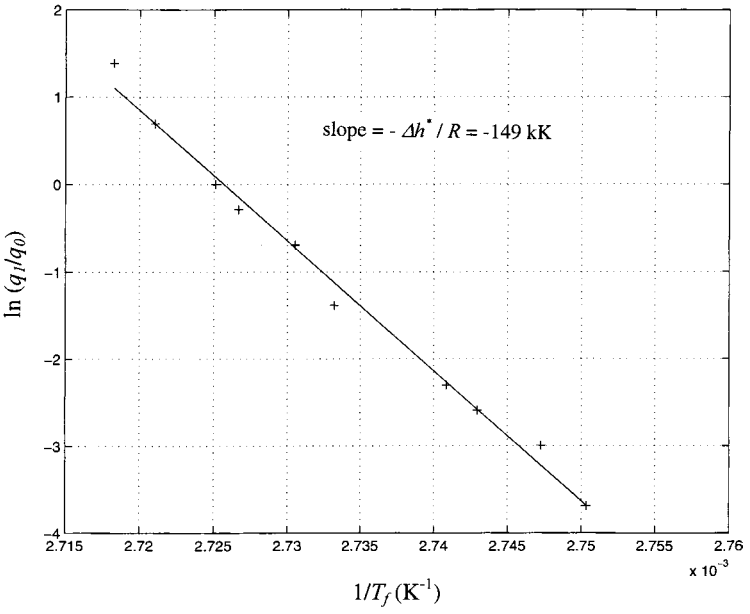

Fig. 3. Well-known construction giving the apparent activation enthalpy, Δh^*, shown for PMMA. T_f is the fictive temperature, q_1 and q_0 are heating and cooling rates, respectively.

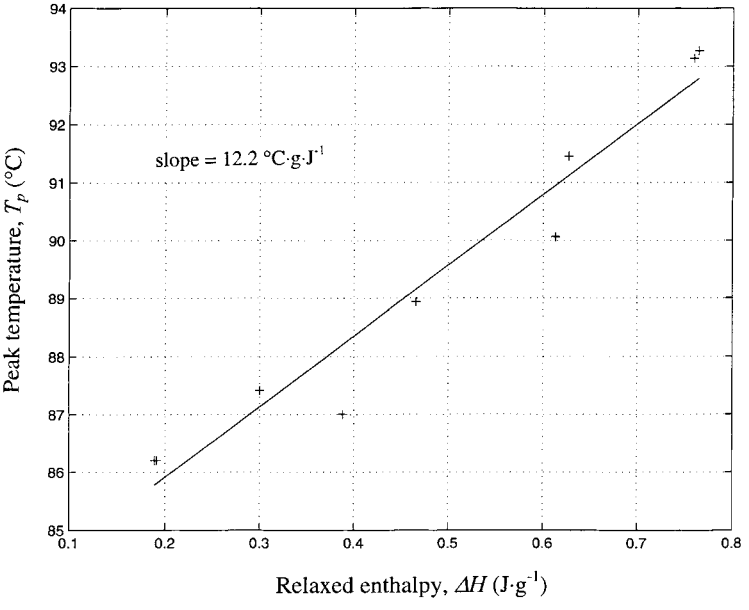

Fig. 4. Peak temperature vs. relaxed enthalpy for 10/90 PEO/*a*-PMMA blend. Towards parameter x using the peak–shift method.

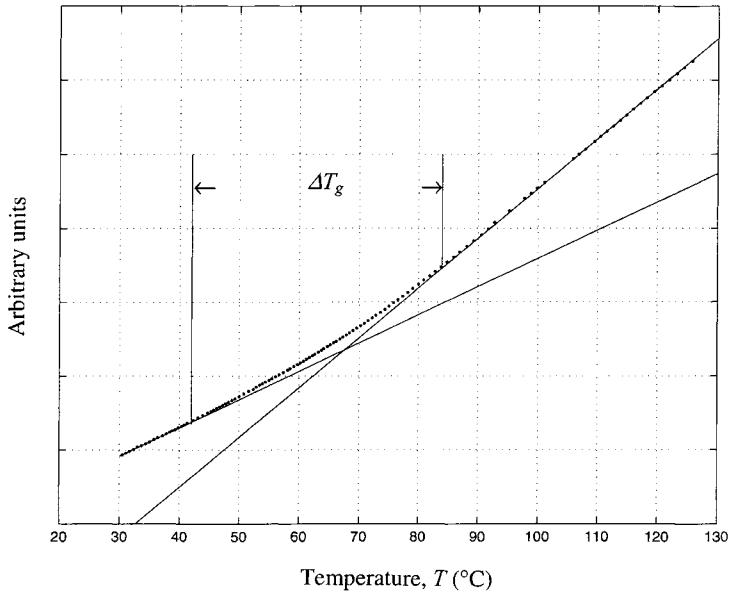

Fig. 5. Volume–temperature diagram for 06/94 PEO/*a*-PMMA blend measured on cooling at a rate of approximately −0.1°C/min. Solid lines represent glassy and liquid asymptotes. ΔT_g represents the width of T_g-region measured between departure points from asymptotes.

function $F(x)$ according to

$$F(x) = \Delta C_p \cdot \frac{\partial T_p}{\partial \Delta H}, \tag{6}$$

where $F(x)$ is approximated by the following equation:

$$F(x) = \left(\frac{1}{x}\right) - 1. \tag{7}$$

Thus, parameter x can be obtained from Eqs. (6) and (7).

The pre-exponential parameter, τ_0, can be calculated from Eq. (3) as shown by Hodge [27] in the following way:

$$\ln \tau_0 = -\frac{\Delta h^*}{R \cdot T_g} + \ln \tau(T_g) \approx -\frac{\Delta h^*}{R \cdot T_g} + 4.6$$
$$[\tau(T_g) \approx 100\,\text{s}]. \tag{8}$$

The relaxation time at the glass transition temperature, $\tau(T_g)$, is assumed to be equal to 100 s; the lower limit of the commonly accepted range of relaxation times at T_g [41].

4.2. Dilatometric results

Fig. 5 shows a temperature sweep (cooling curve) measured with the mercury-in-glass dilatometer for the 06/94 blend at an approximate cooling rate of −0.1°C/min. Similarly, data for 00/100 and 14/86 blends were acquired. The coefficients of cubical thermal expansion (CTE), *a,* were found by following a procedure given in ASTM D864 Standard (18.2×10^{-5} and 1.0×10^{-5} K^{-1} for mercury and glass, respectively). $a_l = 6.10 \times 10^{-4}\,K^{-1}$ and $a_g = 2.11 \times 10^{-4}\,K^{-1}$ for the 06/94 blend in the rubbery and glassy state down to 30°C, respectively, were determined from the slope of the respective asymptotes. Results for all tested blends are given in Table 2. Obtained values compare very well with those from PVT measurements by Schmidt and Maurer [42] who reported $a_l = 6.14 \times 10^{-4}\,K^{-1}$ and $a_g = 2.17 \times 10^{-4}\,K^{-1}$ CTE (average values). CTE data for PMMA are also given by Wunderlich

Table 2
Dilatometric results

Material	00/100	06/94	14/86
$T_{g,vol.}$ (°C)	83	68	48
$\Delta T_{g,vol.}$ (°C)	37	42	51
α_l (K^{-1})	6.07×10^{-4}	6.10×10^{-4}	5.91×10^{-4}
α_g (K^{-1})	2.04×10^{-4}	2.11×10^{-4}	2.76×10^{-4}
$\Delta\alpha$ (K^{-1})	4.03×10^{-4}	3.99×10^{-4}	3.15×10^{-4}

[43]: $5.74 \times 10^{-4}\,K^{-1}$ and $2.53 \times 10^{-4}\,K^{-1}$. For a 50/50 (unspecified) PEO/*a*-PMMA blend, the temperature dependence of a_l is given by Pedemonte et al. [6]. For example, for a temperature of 60°C a value of $6.67 \cdot 10^{-4}\,K^{-1}$ can be found. Schmidt and Maurer [42] reported $a_l = 6.78 \times 10^{-4}\,K^{-1}$ for a 50/50 vol% PEO/*a*-PMMA blend. Also in Table 2, $\alpha_l - \alpha_g = \Delta\alpha$ and the temperature width over which CTE changes, ΔT_g, are given (apart from the 10/90 blend for which case measurements were not made). We note the fairly constant value of α_l, slightly increasing α_g and decreasing $\Delta\alpha$ values, with the increasing amount of PEO in the blend. Somewhat lower $\Delta\alpha$ value for the highest blend is noticed, in agreement with previously mentioned data [42]. Some overestimation of α_g can be expected and the difference is due to not achieving a truly glassy state of constant structure (i.e. of constant fictive temperature) on cooling, a notoriously difficult state to reach. It can be observed in Table 2 that ΔT_g increases with the increasing content of PEO in the blend.

It is accepted as a common laboratory practice that the intersection of the glassy and rubbery asymptotes established at a cooling rate in the range −0.1 to −1°C/min determines the glass transition temperature. Results are summarised in Table 2, where they are denoted $T_{g,vol.}$, and are given for a cooling rate of about –0.1°C/min. According to Kovacs [44] and Struik [45], a T_g value obtained from the intercept of volumetric liquid and glassy asymptotes should be associated with a relaxation time, τ, of about $2.3/q$, where q is the cooling rate in °C/s. In the present case this gives a relaxation time of about 1400 s, which is fairly close to the 100–1000 s range [38], commonly accepted for the glass transition temperature. It can be compared in Tables 1 and 2 that $T_{g,vol.}$ (measured at a lower rate) is always significantly lower than $T_{g,enth.}$ (measured at a higher rate). It can be easily found that this ranking is also true when these temperatures are compared at the same cooling rate. Using the activation energy given in Table 1 we calculate that $T_{g,enth.}$ at a cooling rate of –0.1°C/min is 91.1°C, 76.8°C and 54.7°C for 00/100, 06/94 and 14/86 blends, respectively. Thus, we observe for case I and II that experiments at the cooling rate of –0.1°C were carried out above T_g ($\tau = 1400$ s) (the dilatometric T_g is a lower by 6.7–8.8°C compared to mid-point calorimetric T_g).

Similarly as the enthalpic aging experiments, isothermal volume contraction was carried out at temperatures $T_{g,enth.} - 5$°C and $T_{g,enth.} - 2$°C. Isothermal contraction at $T_{g,enth.} - 5$°C was triggered off by a *T*-jump (carried out at an average cooling rate of about −5°C/min comparable to the cooling rate used in enthalpic and mechanical measurements) following equilibrium at $T_{g,enth.} + 5$°C. This was achieved by a quick replacement of the dilatometer from a hotter bath to a thermostatic bath set to the given aging temperature. Dilatometer was allowed a certain time for thermal equilibration, and then data were recorded. Time t_i required for the equilibration was estimated to be 140 s. This was established from the ''knee'' on the mercury height vs. time plot. It may suffice to mention that several *T*-jumps from several higher temperatures to several lower temperatures were used to establish t_i. Initial departures were significantly less than $\Delta\alpha \cdot (T_{g,enth.} - T_a)$; the value anticipated for an instantaneous *T*-jump of magnitude $(T_{g,enth.} - T_a)$. Isothermal contraction data for 00/100 and 06/94 blends are shown in Fig. 6a.

Isothermal contraction at aging temperature $T_{g,enth.} - 2$°C was carried out differently. Sample in the dilatometer was equilibrated for 1 h at $T_{g,enth.} + 15$°C. Then the temperature of the bath was decreased at an average cooling rate of –0.5°C/min until $T_{g,enth.} - 2$°C was reached. By using this uncommon procedure we hoped to achieve a more uniform and more controlled cooling rate in the sample. Time t_i required for temperature stabilisation in the dilatometer was estimated in the same way as described previously, and was the same (140 s). Contraction data are shown in Fig. 6b. The final approach to equilibrium is included in the inset graph.

4.3. Mechanical results

Samples were annealed for 30–60 min at about $T_{g,enth.} + 30$°C and next were slowly cooled at −1°C/min to a temperature $T_{g,enth} + 5$°C where further annealing for about 5 min took place. Next, *T*-jumps were carried out at a cooling rate of about −10°C/min. Two temperature down-jumps were carried out for each material to the following aging temperatures: $T_{g,enth.} - 6$°C and $T_{g,enth.} - 8$°C (for PMMA), $T_{g,enth.} - 6$°C and $T_{g,enth.} - 9$°C (for 06/94), $T_{g,enth.} - 5$°C and $T_{g,enth.} - 8$°C (for 10/90). Physical

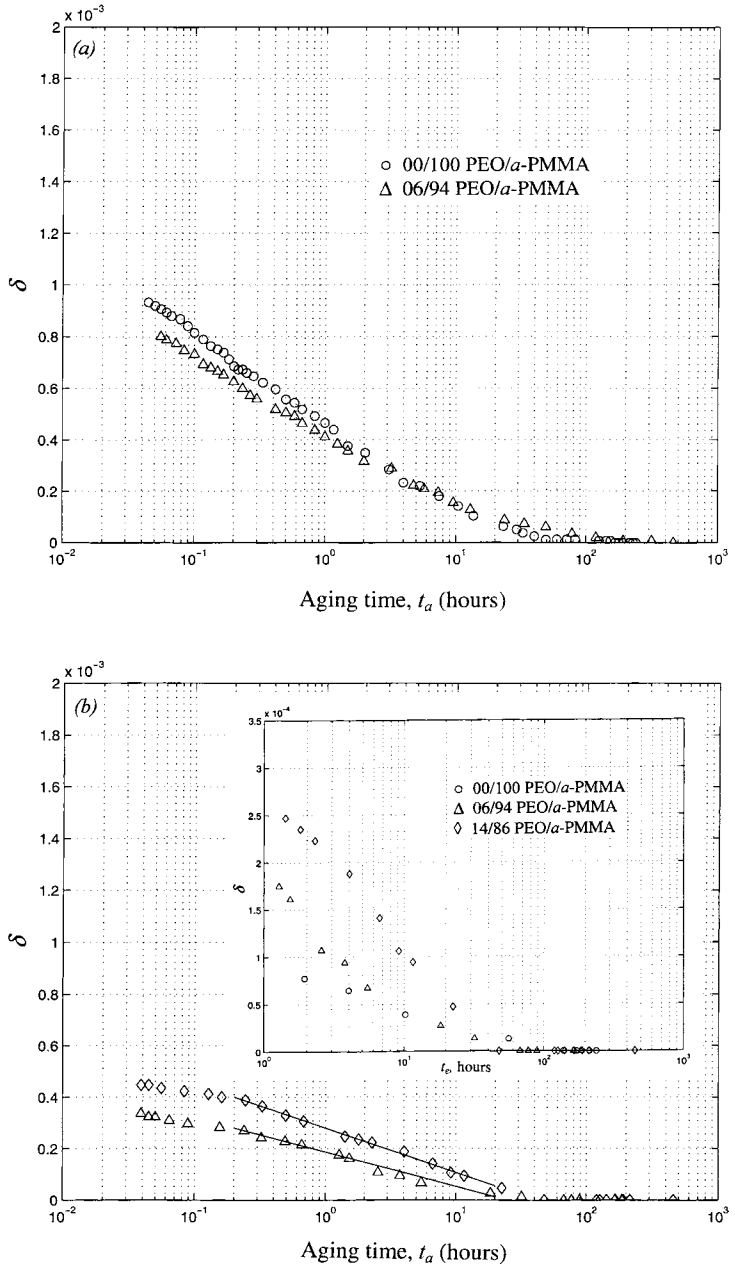

Fig. 6. Isothermal volume contraction of blends at: $T_a = T_{g,enth.} - 5°C$ (a), and $T_a = T_{g,enth.} - 2°C$ (b). Volume is normalised as the relative departure from equilibrium, $\delta = (V - V_\infty)/V_\infty$ where V_∞ denotes the equilibrium value. t_a is the aging time measured from: the beginning of the quench (a), and time at which bath reaches programmed aging temperature T_a (b). Further time, t_i, was allowed for the sample to reach programmed aging temperature (this time was 140 s in both cases). Points shown in the figures represent isothermal contraction.

aging data by DMA were recorded for all above cases. For the 06/94 blend, additional aging data at $T_{g,enth.} - 6°C$ were obtained by stress relaxation. Somewhat varying aging temperatures, different from the assumed $T_{g,enth.} - 5°C$ level, was caused by the difficulty in realising the pre-programmed temperature

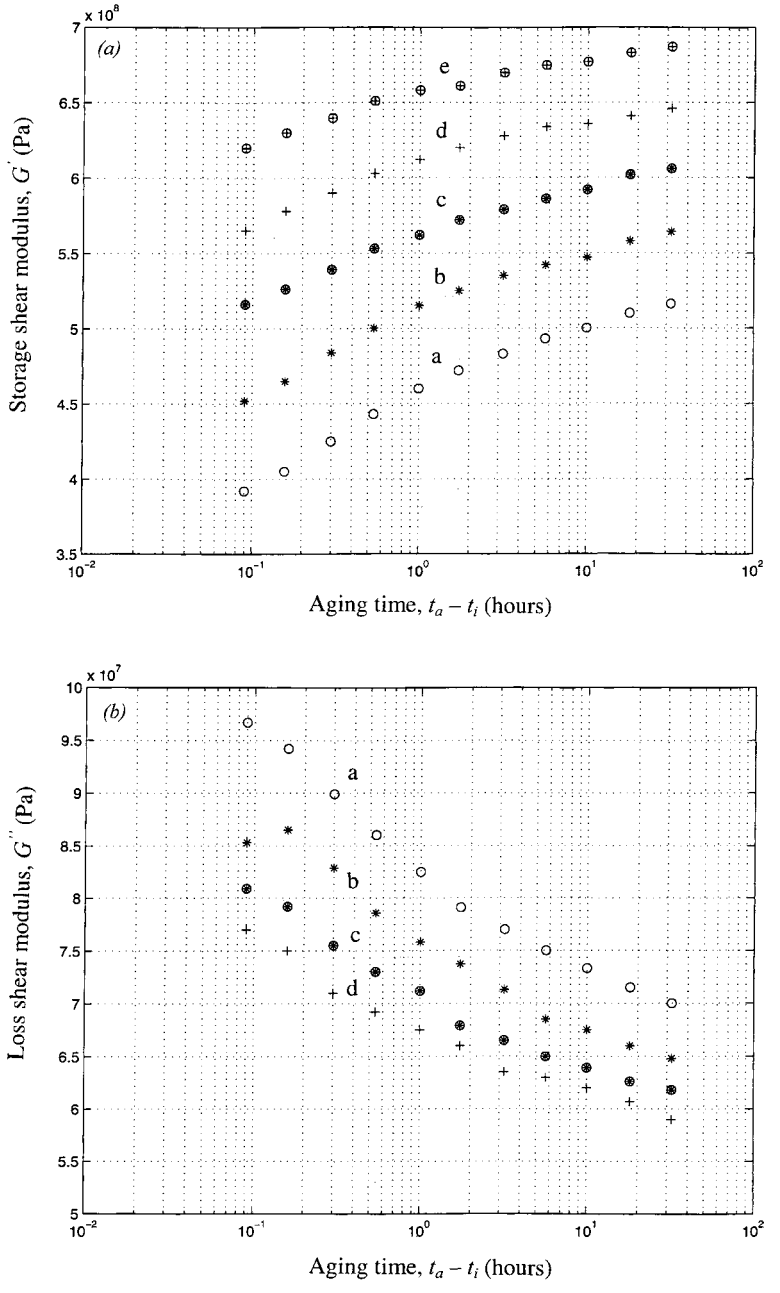

Fig. 7. Evolution during physical aging of: (a) storage shear modulus, G', and (b) loss shear modulus, G'', for PMMA following a down-jump from $T_{g,enth.} + 5°C$ to $T_{g,enth.} - 6°C$. Time is measured from t_i, with $t_i = 45$ s needed for temperature stabilisation $\pm 0.1°C$. Frequencies (Hz) are: 0.1 (a), 0.314 (b), 1.0 (c), 3.14 (d) and 10 (e).

history. The instrument's option for zero axial force was used to assure pure torsional loading.

As an example, the storage shear modulus, G', and the loss shear modulus, G'', for 00/100 blend, at selected frequencies between 0.1 and 10 Hz, vs. the aging time is shown in Fig. 7. As can be seen G' monotonically increases (Fig. 7a) and G'' monotonically decreases (Fig. 7b) with the increasing aging

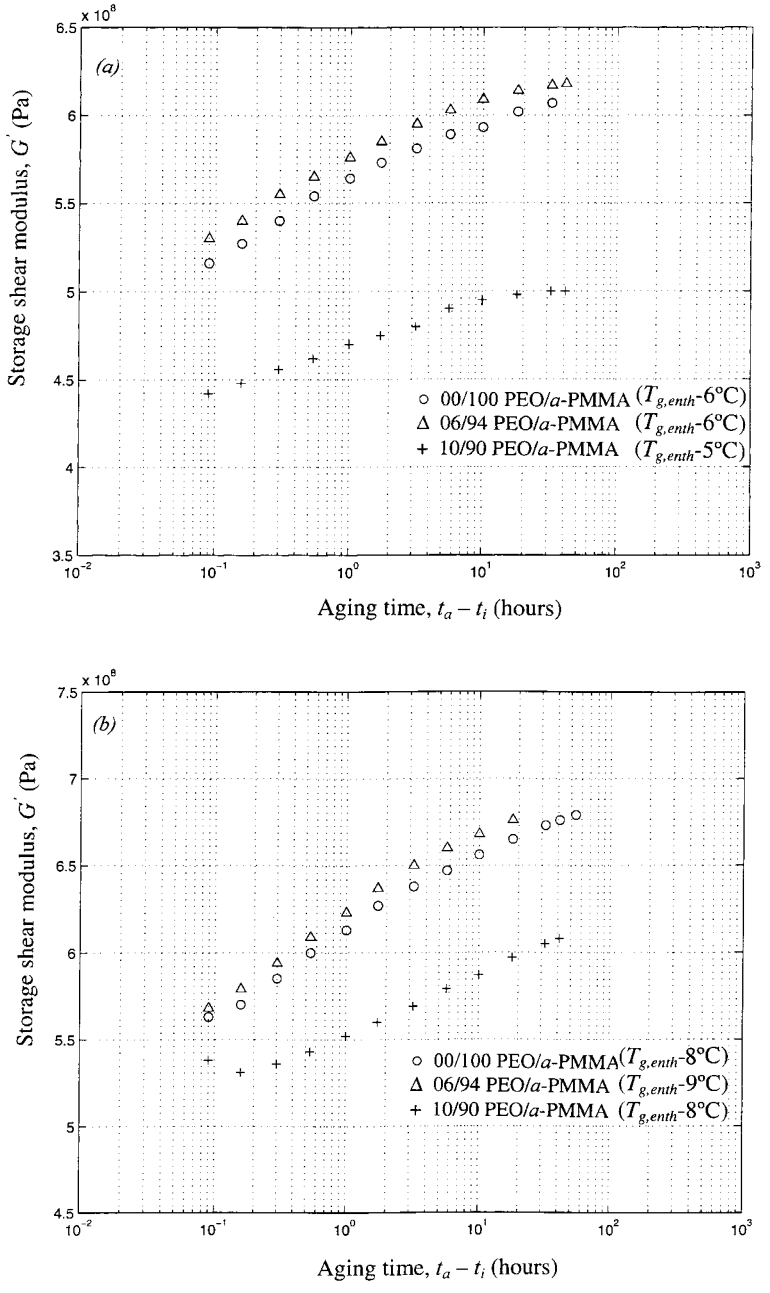

Fig. 8. Evolution during physical aging of the storage shear modulus, G', following a down- jump from equilibrium to indicated temperatures. Frequency = 1 Hz. Time is measured from t_i, with $t_i = 45$ s needed for temperature stabilisation ± 0.1°C.

time, in agreement with the behaviour of polymer glasses reported in the literature. Monotonically increasing G' with the increasing aging time was obtained for all tested blends, for both aging temperatures (see Fig. 8a and b). There, it can be seen that highest G' values were obtained for the 06/94 blend (open triangles). Schmidt and Maurer [42], from their PVT measurements, have also noted a minimum in the

Table 3
Storage modulus, G', at 60°C

Material	00/100	06/94	14/86
Modulus G', MPa at 1 Hz	888	902	227

isothermal compressibility, i.e. a maximum in the bulk modulus, at room temperature as well as at 110°C and 130°C for a composition near to 10 vol% PEO. This behaviour was also reported by Chang [14] and Chang et al. [15] who measured a slightly higher relaxational modulus for mixed in solution PEO/*a*-PMMA blend compared to the *a*-PMMA polymer. This was measured by these authors at a relatively lower temperature and in a blend with a higher content of PEO. A higher stiffness for this blend was also measured by us at 60°C (see Table 3). There, a slight increase of G' for 6 vol% PEO followed by a sharp decrease of G' can be seen.

Proceeding from G' data, the aging rate μ was calculated (Eq. (9))

$$\mu = \frac{-\mathrm{d}\log(\omega/\omega_\mathrm{r})}{\mathrm{d}\log(t_\mathrm{a}/t_\mathrm{ar})}, \tag{9}$$

where ω_r and t_ar denote the reference frequency and aging time. The procedure is described elsewhere [33]. Isochronal lines and master curve obtained by time-aging time superposition using purely horizontal shifting is shown for PMMA, as an example, in Fig. 9a and b. The shift factor, log a, vs. normalised aging time, $t_\mathrm{a}/t_\mathrm{ar}$, for both discussed temperatures is represented in Fig. 10a and b, for all measured blends. For larger *T*-jumps, approximately greater than 13°C, the time-aging time superposition failed and master curves by horizontal shifting were not well formed (not included). To confirm the aging rate by G' data, torsional stress relaxation curves measured on aging were shifted horizontally to form a master curve. Measurements were made only for the 06/94 blend. Stress relaxation plots and time-aging time superposition is shown in Fig. 11a and b, respectively. As for G' previously, only a horizontal shift (change of mobility) was sufficient to obtain a highly satisfactory master curve. An aging rate of 0.41 was obtained. This compares fairly well with the value of 0.38 measured by DMA.

The aging rate vs. composition, for the two aging temperatures, is shown in Fig. 12. The distance to

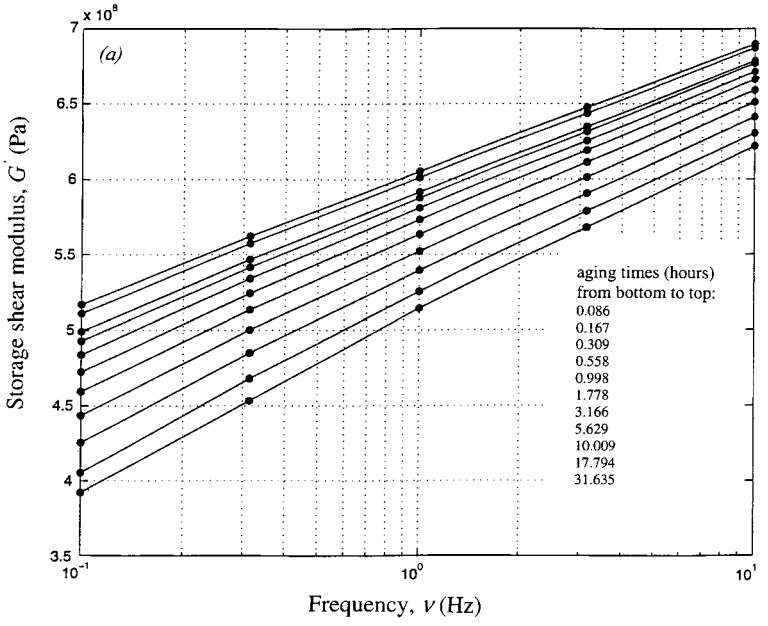

Fig. 9. (a) Constant aging time (isochronal) lines for the storage shear modulus G' from the aging experiments represented in Fig. 7 (aging times are given in the inset table). (b) Time-aging time superposition (master curve) for the isochronal lines represented in Fig. 9a. Master curve was formed by horizontal shifting to the isochronal line at 0.086 h.

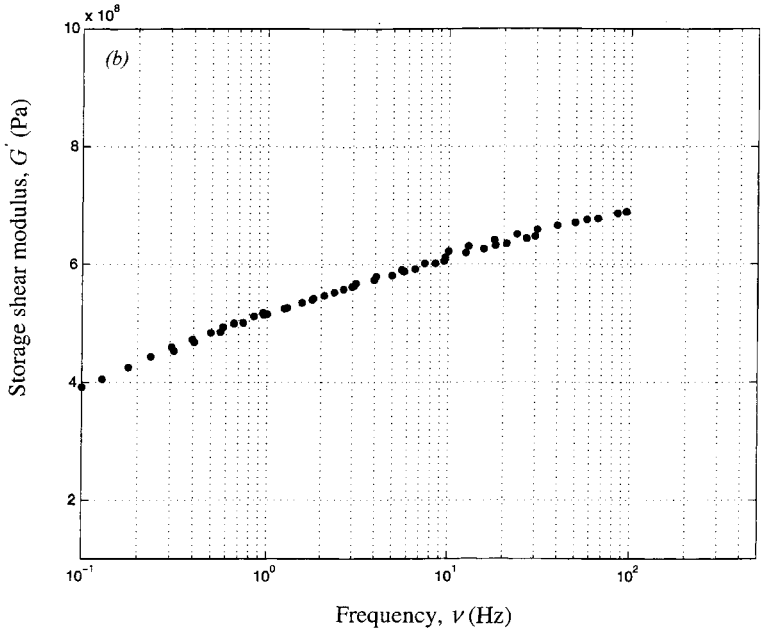

Fig. 9. (*Continued*).

$T_{g,enth.}$ slightly varied as explained in the caption of Fig. 12, but this had no major influence on the observed trend. It can be seen that the aging rate monotonically decreases with the increasing content of PEO, and aging rates at the higher aging temperature are lower. The decreasing aging rate with the

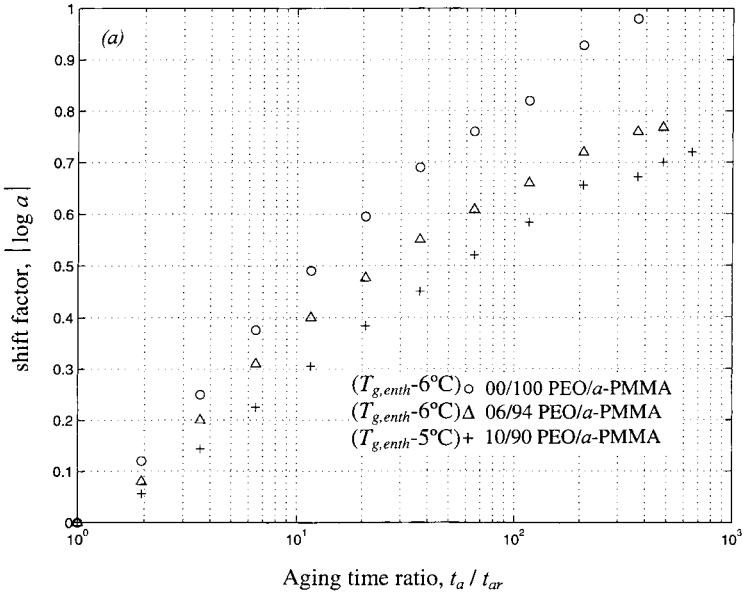

Fig. 10. log (shift factor) vs. aging time ratio (in log scale) evaluated from the frequency dependence of storage shear modulus, G', at different aging times after a quench from approximately $T_{g,enth.} + 5°C$ to indicated temperatures. In figure (a) aging temperatures are fairly close to $T_{g,enth.} - 5°C$, and are lower for the cases represented in figure (b).

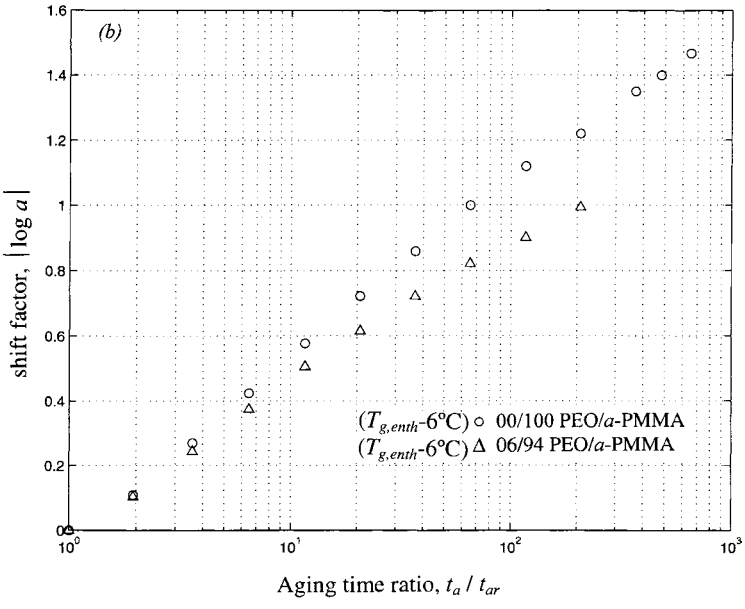

Fig. 10. (*Continued*).

increasing content of PEO is different from the result of Chang [14] who measured aging rates for pure *a*-PMMA and 15/85 wt% PEO/*a*-PMMA, and found that the aging rate for the *a*-PMMA is lower than that of the blend. However, the author used a different from ours thermal history and sample preparation technique

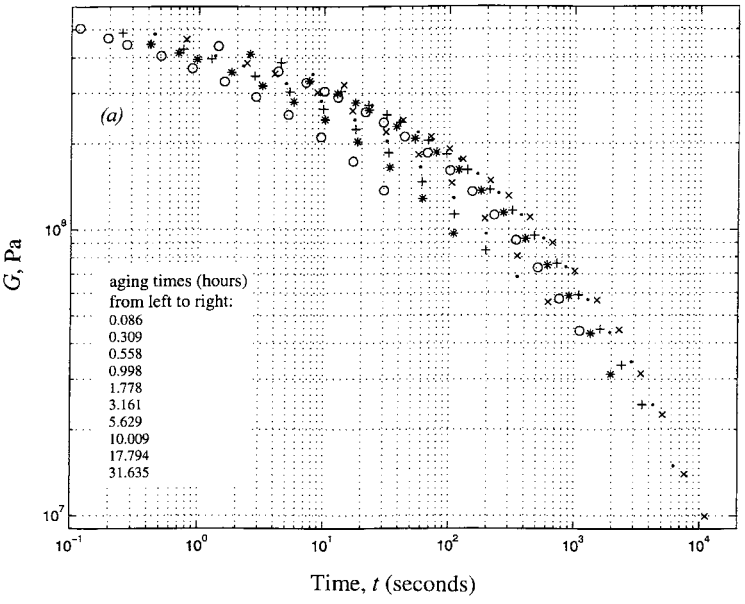

Fig. 11. (a) Shear modulus in stress relaxation of 06/94 PEO/*a*-PMMA blend aged at $T_{g,enth.} - 6°C$. The modulus was determined at specific aging times after the quench (given in the inset table). (b) Time-aging time superposition for the curves in figure (a). The master curve was formed by horizontal shifting to the aging time of 31.635 h.

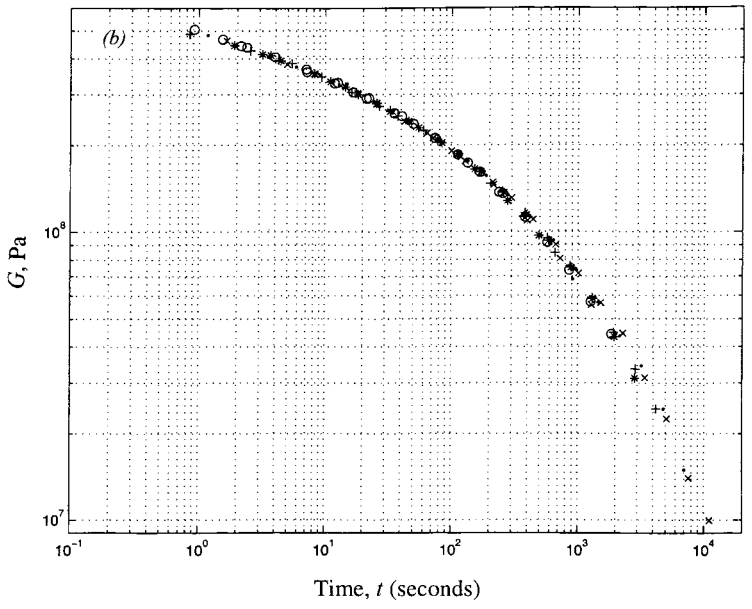

Fig. 11. (*Continued*).

(mentioned before). Thus, we applied the same thermal history, namely, PMMA samples (the same grade as used in this work) were annealed at $T_{g,enth.} + 8°C$ for 1 h and quickly quenched (at $q = -60°C/min$) to a temperature of $T_{g,enth.} - 9°C$. An aging rate of 0.53 comparing to approximately 0.58 measured by

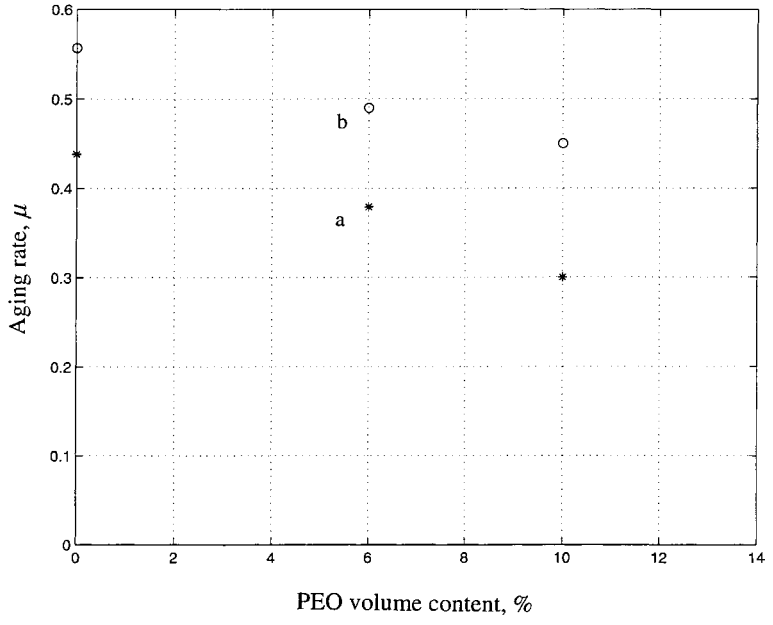

Fig. 12. Aging rate vs. composition. Plots (a) and (b) were constructed from data in Fig. 10a and b, respectively.

Chang was obtained. We discuss this in the following section.

5. Discussion

5.1. Experimental error and other sources of uncertainty

$x = 0.4$ measured by us for PMMA at $T_{g,enth.} - 5°C$ (see Table 1) is higher than the value of 0.2 reported by Hodge [27] but is in fair agreement with the value of 0.37 reported by Hutchinson [19]. Perhaps the difference can be explained by the fact that the peak–shift method used by us often seems to give larger values of x than does the curve-fitting method used by Hodge. Tribone et al. [18] measured x values for PMMA between 0.15 and 0.40. We consider $x = 0.28$ and 0.23 measured by us for PMMA and 06/94 blend, respectively, at $T_{g,enth.} - 2°C$ as being too low. Such low values were caused most likely by not reaching the limiting condition in the peak–shift method, and were not analysed. Δh^* measured by us for PMMA is in agreement with the result given for PMMA by Hodge [27]. On the other hand, this value contrasts with 870 kJ/mol reported by Hutchinson [19]. We discuss Δh^* further ahead in Section 5.3. There is a rather large experimental scatter in enthalpic data on aging which is typical for this type of measurements. This gives an uncertainty of ± 0.06 for x, whereas the uncertainty of the apparent activation enthalpy is estimated to be $\pm 10\%$, in agreement with Hodge [27]. The width of glass transition region, ΔT_g, increased with the increasing PEO content. This can be seen in Table 2 and Fig. 1 where volumetric and calorimetric measurements are presented. It is shown in Table 1 that the specific heat capacity difference, ΔC_p, decreased. According to Shalaby and Bair [46], the increasing width of the T_g-region in a blend can be interpreted as onsetting phase separation. As proposed by above authors, the loss in ΔC_p is caused by large and diffused interfacial regions that cannot be detected by DSC. Broadening of the T_g-region and the decrease of ΔC_p with the increasing PEO content in the blend has an influence on measured relaxed enthalpy. It is not clear to us whether this reflects real material behaviour or is an effect from the changing shape of the thermograms.

The use of the TNM model for polymer blends has been discussed in the past. For example, Cowie and Ferguson [30] found it impossible to obtain reasonable prediction of C_p data for enthalpy relaxation of a 50/50 wt% miscible blend of poly(vinyl methyl ether) (PVME) and polystyrene. The reason was believed to be in the broadening of the glass transition region for the blend. Prediction of enthalpy relaxation in polymer blends using the TNM model has also been analysed by Oudhuis and ten Brinke [21] who concluded that relaxation can be considerably influenced by the presence of concentration fluctuations (width of T_g-region).

5.2. Enthalpic and volumetric relaxation

We discuss separately case I (cooling at $-7.5°C$/min, followed by aging at $T_{g,enth.} - 5°C$) and case II (cooling at $-0.5°C$/min, followed by aging at $T_{g,enth.} - 2°C$) results. In Fig. 2a, increasing relaxed enthalpy with the increasing aging time is shown. Such behaviour is expected. It is difficult to comment on the relative position of plots. The spread of data must be taken into account. Nevertheless, it is seen that data for the 10/90 blend are lower than that of 06/94 blend, for the same aging times. This trend is in agreement with results shown by Oudhuis and ten Brinke [21], and Cowie and Ferguson [30] for other miscible blends of dissimilar polymers. In particular, it is difficult to compare ΔH data for PMMA and 06/94 blend as differences are very close or within experimental error. It could be argued that the 06/94 blend departs more from equilibrium due to its higher stiffness (see Fig. 8), as explained by Tangpasuthadol et al. [47].

It can be calculated using the activation enthalpy given in Table 1, that the glass transition temperature for 00/100 and 06/94 blends at the cooling rate of $-0.5°C$/min is 92.6°C and 78.7°C, respectively. Thus at $T_{g,enth.} - 2°C$ in both materials, we are above the T_g for the cooling rate used (by 0.4°C and 1.3°C, respectively), and it should be expected that the change of ΔH will be very small. This is just what we see in Fig. 2b for PMMA, where it is even uncertain to assume any increase. For 06/94 blend (in the same figure) ΔH values are higher than that of PMMA and the difference is increasing with the increasing aging time, and thus it is seen that relaxation in PMMA is on the whole

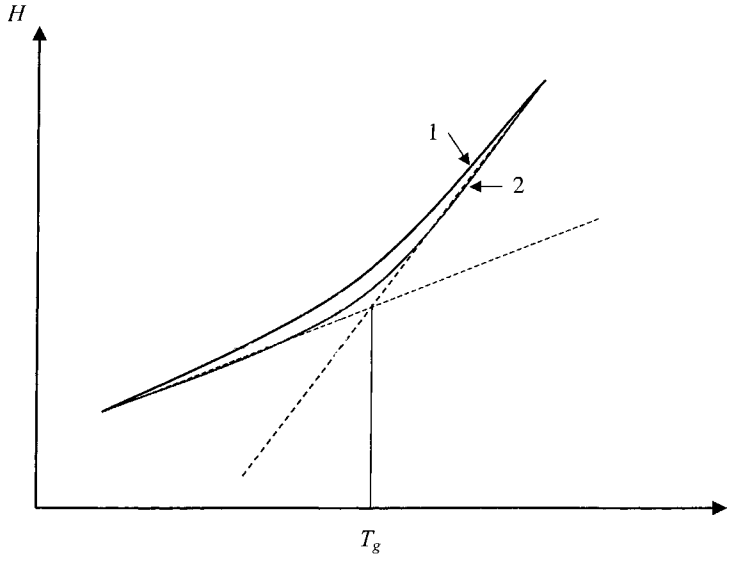

Fig. 13. Interpretation of enthalpy relaxation at various temperatures in the glass transition region. Lines 1 and 2 schematically represent behaviour of 06/94 and 00/100 materials, respectively. For simplicity, different T_g for these two materials are brought into coincidence. At the same temperature distance to T_g the excess enthalpy in material 1 is higher. This is due to the more spread out transition interval.

less hindered, and a state resembling equilibrium is quickly reached. A following explanation is offered (see Fig. 13). Schematically, line 1 represents 06/94 blend with a broader glass transition, and line 2 represents PMMA with a narrower one. For simplicity T_g values are brought into coincidence. It can be accepted that the excess enthalpy just above T_g is less in PMMA compared to 06/94 blend. Dilatometric data in Table 2 confirm this. Transition in 06/94 blend is broader than that in PMMA. Possibly, this is also manifest as a smaller endothermic peak (shown by 14/86 in Fig. 1b). Broad transition implies retarded transition, hence even at this relatively high aging temperature equilibrium is not reached after 20 h and most likely even after 30 h (Fig. 2b). After this explanation we summarize cases I and II. For aging below enthalpic T_g (case I) for the cooling rate used, we observe that ΔH values and the rate of relaxation both decrease when PEO is increased from 6 to 10 vol%, whereas above the enthalpic T_g (case II) the opposite is true when PEO is increased from 0% to 6%. However, as can be compared in Fig. 2, not all data follow this relaxational behaviour.

Now the isothermal volume contraction data are analysed. Similarly as before in cases I and II, $T_{g,enth.} - 5°C$ and $T_{g,enth} - 2°C$ aging temperatures are used. Results for the 00/100 and 06/94 blends following the larger T-jump at a cooling rate of –5.0°C/min are shown in Fig. 6a. The cooling rate is close to the one used for calorimetric measurement and we can assume, similarly as for the enthalpic measurements, that aging temperatures are lower than $T_{g,enth.}$ for the cooling rate used. This is not the same when $T_{g,vol.}$ is considered. We may suppose that a ratio of 50 in cooling rates ($-0.1 \rightarrow -5.0$°C/min) might increase $T_{g,vol.}$ by 6°C or 7°C, from 83°C for PMMA and 68°C for 06/94, say to 90°C and 75°C, respectively. Thus, in both experiments the materials were aged at 90°C and 77°C, that is at $T_{g,vol.}$ and above, for the cooling rate used. It can be seen in Fig. 6a that the measured timescales are apparently of the order of hundreds of hours, and the initial departure is close to $\delta = 1 \times 10^{-3}$. Thus, in spite of the closeness to $T_{g,vol.}$ significant aging takes place. The enthalpic timescales were not measured, but we may suppose that they are longer when measured at the same temperature, due to the larger negative temperature distance to the enthalpic T_g. Consequently slower enthalpic relaxation can be assumed. We observe in Fig. 6a that the initial departure from equilibrium for the 06/94 blend is

lower than that of PMMA, what can be explained by the relatively to $T_{g,vol.}$ higher aging temperature, and the relaxation rate is lower (particularly after aging for several hours) and the timescale for equilibrium is longer. Thus, following a similar temperature history, we observe the same trend in dilatometric aging behaviour as in the previously discussed enthalpic data.

Volume contraction data following the $T_{g,enth.} - 2°C$ temperature jump are shown in Fig. 6b. Similarly as discussed above, it is pertinent to place the relaxation relative to T_g. It can be found that $T_{g,vol.}$ at the cooling rate of $-0.5°C$ is about 86°C, 71°C and 51°C for the 00/100, 06/94 and 14/86 blends, respectively, that is aging at $T_{g,enth.} - 2°C$ is actually 7–9°C above respective volumetric T_g, and is very close to $T_{g,enth.}$ for this low cooling rate. As can be expected, initial departure from equilibrium is very small due to the relatively high temperature exceeding T_g. This explains the high scatter. Nevertheless, varying departures, timescales and relaxation rates can be noted (for clarity only two complete plots are represented; the final approach to equilibrium is shown for all measured cases). The inflectional rate was determined over an extended inflectional region (shown with a solid line) rather than for an inflection point. It is a rather straightforward case to explain the behaviour shown in Fig. 6b. Far above T_g any significant volume relaxation can be expected only if the glass transition interval is broad. Fig. 6b shows just this: initial excess volume d is about 0.3×10^{-3} for 06/94 blend and is higher (significantly more than 0.4×10^{-3}) when the content of PEO is increased to 14 vol% implementing a broadened transition (see ΔT_g in Table 2). However, in contrast to the behaviour close to $T_{g,vol.}$ observed in Fig. 6a, and in contrast to what we should expect from the broadening of the T_g interval, the timescale decreases and the inflectional relaxation rate increases with the increasing PEO content. This behaviour was observed for all three materials with PEO content between 0 and 14 vol%. Thus we note a contrasting behaviour. Enthalpic and volumetric relaxations for PEO/PMMA blends relaxing below $T_{g,enth.}$ are different from these taking place at higher temperatures very close to $T_{g,enth.}$. Although the analysed difference in aging temperatures was small, apparently it influenced the physical aging behaviour in the $T_{g,enth.}$-region.

5.3. Application of the TNM parameters

To start with, we discuss the difficulty encountered when attempting to calculate the β parameter for the blends. The relaxed enthalpy in equilibrium, ΔH_∞, is needed for calculation of β. Experimental acquisition of ΔH_∞ is generally rather difficult. There is notoriously a high and increasing with the increasing aging time scatter in ΔH values. In-instrument aging is a good option towards a lower scatter, but then much shorter times are available for aging. As shown in Fig. 2, equilibrium for the blends was not attained even at relatively high aging temperatures. Also, resolution of the instrument (in this case the calorimeter) has an influence on the measurement. Higher ΔH_∞ must be expected with an instrument with a higher resolution. It is possible to calculate ΔH_∞ based on the assumption of temperature independent specific heats in solid and liquid states (co-linear liquidus lines), that is by extrapolation. We include such values calculated at $T_{g,enth.} - 5°C$ in Table 1, there denoted $\Delta H_{\infty,extra}$, for completion. However, extrapolation with a straight line is approximate; this in particular is the case for enthalpy relaxation where deviation from a linear equilibrium enthalpy regression is particularly pronounced. It can also be analysed, that apart from the case of equilibrium at 0 K, ΔH_∞ is predicted only for $t = \infty$. To summarize, we found it difficult to establish an acceptable ΔH_∞ value, and thus parameter β was not calculated.

The pre-exponential parameter τ_0 was calculated from Eq. (8) and results are given in Table 1. Values are impractically small compared to any known physical timescale, and are not considered further.

Δh^* and x parameters can be obtained independently and separately, without involving any of the Eqs. (1)–(4). We can then refer to Δh^* and x as input parameters. The four TNM parameters form a unique set, that is a change of any one parameter cannot be compensated by adjusting another one. It is attractive to obtain these parameters without involving some uncertainties associated with the two remaining parameters β and τ_0(discussed earlier). Parameter $\theta\cdot(1-x)$ can be calculated from the input parameters Δh^* and x. It has been shown for several amorphous polymers and an inorganic glass that $\theta\cdot(1-x)$ characterises the inflectional volume and enthalpy relaxation rate which decreases with the increasing $(1-x)\cdot\theta$ (Málek and

Montserrat [39]). Results for $(1-x)\cdot\theta$are included in Table 1. The three parameters x, Δh^* and $(1-x)\cdot\theta$are discussed in the following section.

Physical interpretation attached to any of the TNM parameters is a vexed question. Nevertheless, it is commonly accepted that β characterises the width of distribution of relaxation times. Low β implies a broad distribution. In turn, a wide distribution can be associated with greater cooperativity expressed as interaction between individual relaxing units and their surroundings. As explained earlier, we did not calculate β due to the uncertainty in assuming the ΔH_∞ value. It has been also discussed, that τ_0 values obtained for the blends are unphysically small, and thus are not analysed. A molecular interpretation of x and Δh^* has been advanced by Hodge [48], given by the author for unblended polymers. Δh^* is considered by the author in terms of degree of cooperativity and, alternatively, an energy barrier that must be exceeded during structural relaxation, and the decreasing Δh^* activates less energy demanding relaxation. We note an objection raised by Struik [45] with respect to any generalisation of the Arrhenius formalism, in particular, any attempt to describe non-Arrhenius behaviour with an apparent value of activation energy defined as the slope of ln τ vs. $1/T$ curve, in the case of mechanical and dielectric relaxations. Parameter x is considered by Hodge as a measure of the relative importance of the temperature and the structure in determining the average relaxation time, and is interpreted by the author in terms such as chain conformations and their correlations, and smaller x implies more cooperativity. $(1-x)\cdot\theta$is a combination of x, T_g, Δh^* and R, and may be regarded as a quantity capturing structural mechanisms (co-operativity) and relaxation kinetics at the inflection point.

It can be seen in Table 1 for case I that a significantly higher x indicating lower molecular co-operativity is obtained for PMMA compared to the blends. Also, on the whole, $\theta\cdot(1-x)$ increases with the increasing PEO content indicating that the increasing amount of PEO hinders relaxation, in agreement with the obtained experimental results. Thus, we conclude that the increasing content of PEO up to 14 vol% in the blends gives higher structural co-operativity and hinders structural relaxation. On the other hand, an expected increase of Δh^* with the increasing content of PEO is not observed. Instead, a non-monotonic behaviour is seen, and it is pertinent to ask why. It can be analysed from Fig. 3, as an example, that Δh^* was determined for a fictive temperature interval of about 5 K by drawing the best straight line through nine points. However, a lower value of Δh^* would be obtained by interpolating a narrower temperature interval corresponding to lower T_f, and a higher Δh^* value would be obtained corresponding to higher T_f. Thus, the data shown in Fig. 3 should not be interpolated with a straight line giving a constant (apparent) Δh value used with the Arrhenius formalism. Similar observation can be made with regard to all blends. This is not surprising taken into account that data were collected in the T_g-region.

5.4. Aging rate behaviour

Aging rate vs. PEO content behaviour for two aging temperatures approximately 5°C and 8°C below $T_{g,enth.}$ (plots a and b, respectively) is shown in Fig. 12. A decreasing rate with the increasing PEO content can be seen for both aging temperatures, although the plots are slightly different, with a non-synergistic variation of the aging rate vs. composition (plot a), and an almost linear variation for the lower aging temperature (plot b). That is, for the higher aging temperature, the aging rate for higher PEO contents becomes smaller than that predicted linearly (simple additivity) from compositions in the lower PEO range. However, it is possible that this is caused by a smaller distance to $T_{g,enth.}$ for the 10/90 blend. The lower aging rate (plot a) at the higher aging temperature is expected. The decreasing aging rate with the increasing PEO content we explain first of all in terms of structural mobility. It can be analysed, for example from Eq. (9), or any other equation defining the aging rate, that μ is a measure of change of mobility manifest as a horizontal shift of a given viscoelastic plot, log a. Then, a material with lower μ is a material in which the state of non-equilibrium changes less during a given time. In equilibrium where $\mu = 0$ there is no change of state and thence no change of mobility. Thus we assume from the plots shown in Fig. 12, within the inaccuracy caused by different distances to the glass transition temperature, that the changing state of non-equilibrium is less in blends with more PEO, and this is just what we should expect when the segmental co-operativity is increased.

An opposite trend in μ was shown in the work of Chang [14]. From the μ data following a high cooling rate obtained by Chang and confirmed by us, we can conclude that possibly the different blend preparation techniques used by us and that author may have caused the opposite trends.

6. Final remarks

Thus from the experimental measurements and the analysis of selected TNM parameters we observe for PEO/*a*-PMMA blends with low PEO content that overall segmental co-operativity is increased by the addition of PEO. Also, we find that volume and enthalpy relaxation and the change of molecular mobility is hindered by PEO. This takes place in blends analysed in the T_g-region just above the volumetric T_g (corresponding to a relaxation time of about 1400 s) but below the enthalpic T_g (measured by midpoint construction, at a cooling rate of –7.5°C/min). Structural co-operativity and relaxation behaviour summarized above is the same as concluded by Chang [14] for samples prepared in a different way, although physical aging rate behaviour in the work of the above author is different from ours. In our work the aging rate is identified as mobility change, and it is possible to reconcile the aging rate behaviour with co-operativity and relaxation behaviour.

The increase of structural co-operativity and decrease of relaxation and mobility change with the increasing PEO content in PEO/PMMA blends aged at $T_{g,enth.} - 5$°C can be regarded as the macrolevel manifestation of onsetting density fluctuation and UCST-type miscibility leading to phase separation. Broadening of the glass transition region with the increasing PEO content has been repeatedly measured by us. Spinodal phase separation in PEO/*a*-PMMA blends prepared in the same way as studied here, has been recently confirmed by Maurer and co-authors [10] from microlevel investigations at a higher PEO content. We believe this explains also the behaviour of the blend at lower PEO content. Thus, we regard the blend as showing immiscible behaviour during physical aging in the solid state. Similar investigations at temperatures very close to $T_{g,enth.}$ showed opposite behaviour, although not all experiments were possible to carry out. This contrasting behaviour, it may be accepted, is just what we should expect close to $T_{g,enth.}$ where in the melt the blend becomes completely miscible.

Acknowledgements

The financial support of the Swedish Board for Engineering Sciences (TFR) is gratefully acknowledged. We are indebted to Prof. J.M. Hutchinson of Aberdeen University for his valuable comments and additions. We thank visiting students Fabrice Balitrand and Vincent Guérin for some dilatometric and enthalpic measurements, and Simon Niederhauser for stress relaxation measurements.

References

[1] L.C.E. Struik, L.C.E., Physical Aging in Amorphous Polymers and Other Materials, Elsevier, Amsterdam, 1978.
[2] X. Li, S.L. Hsu, J. Polym. Sci. B 22 (1984) 1331.
[3] G. Ramana Rao, C. Castiglioni, M. Gussoni, G. Zerbi, E. Martuscelli, Polymer 26 (1985) 811.
[4] T.P. Russel, H. Ito, G.D. Wignall, Macromolecules 21 (1988) 1703.
[5] S. Cimmino, S.E. Di Pace, E. Martuscelli, C. Silvestre, Makromol. Chem. 191 (1990) 2447.
[6] E. Pedemonte, V. Polleri, A. Turturro, S. Cimmino, C. Silvestre, E. Martuscelli, Polymer 35 (1994) 3278.
[7] S. Shimada, O. Isogai, Polym. J. 28 (1996) 655.
[8] C. Wästlund, F.H.J. Maurer, J. Radioanal. Nucl. Chem. 211 (1996) 269.
[9] C. Wästlund, F.H.J. Maurer, Macromolecules 30 (1997) 5870.
[10] C. Wästlund, M. Schmidt, S. Schantz, F.H.J. Maurer, Polym. Eng. Sci. 38 (1998) 128.
[11] S. Schantz, Polym. Mater. Sci. Eng. 71 (1994) 209.
[12] S. Schantz, Macromolecules 30 (1997) 1419.
[13] A.V. Vannikov, J. Vernel, E.I. Mal'tsev, V.V. Savel'ev, R.W. Rychwalski, Polym. Eng. Sci. 39 (1999) 261.
[14] G.W. Chang, Physical aging in the mechanical properties of miscible polymer blends, Ph.D. Thesis, Department of Macromolecular Science, Case Western Reserve University, USA, 1993.
[15] G.W. Chang, A.M. Jamieson, Z. Yu, J.D. McGervey, J. Appl. Polym. Sci. 63 (1997) 483.
[16] J.M. Hutchinson, C.B. Bucknall, Polym. Eng. Sci. 20 (1980) 173.
[17] R. Greiner, F.R. Schwarzl, Rheol. Acta 23 (1984) 378.
[18] J.J. Tribone, J.M. O'Reilly, J. Greener, Macromolecules 19 (1986) 1732.
[19] J.M. Hutchinson, Thermochim. Acta 324 (1998) 165.
[20] T. Sato, K. Katayama, T. Suzuki, T. Shiomi, Polymer 39 (1998) 773.

[21] A.A.C.M. Oudhuis, G. Ten Brinke, Macromolecules 25 (1992) 698.
[22] K. Takahara, H. Saito, T. Inoue, Polymer 40 (1999) 3729.
[23] G. Williams, D.C. Watts, Trans. Faraday Soc. 66 (1970) 80.
[24] A.Q. Tool, J. Am. Ceram. Soc. 29 (1946) 240.
[25] C.T. Moynihan, A.J. Easteal, M.A. deBolt, J. Tucker, J. Am. Ceram. Soc. 59 (1976) 12.
[26] O.S. Narayanaswamy, J. Am. Ceram. Soc. 54 (1971) 491.
[27] I.M. Hodge, J. Non-crystalline Solids 169 (1994) 211.
[28] J.M. Hutchinson, Prog. Polym. Sci. 20 (1995) 703.
[29] J.M.G. Cowie, R. Ferguson, Polym. Commun. 27 (1986) 258.
[30] J.M.G. Cowie, R. Ferguson, Macromolecules 22 (1989) 2312.
[31] G.B. McKenna, M.G. Vangel, A.L. Rukhin, S.D. Leigh, B. Lotz, C. Straupe, Polymer 40 (1999) 5183.
[32] A.J. Kovacs, J.M. Hutchinson, J.J. Aklonis, in: P.H. Gaskell (Ed.), The Structure of Non-crystalline Materials, Taylor and Francis, London, 1977.
[33] M. Delin, R.W. Rychwalski, J. Kubát, C. Klason, J.M. Hutchinson, Polym. Eng. Sci. 36 (1996) 2955.
[34] S.J. Clarson, K. Dodgson, J.A. Semlyen, Polymer 26 (1985) 930.
[35] A. Shefer, M. Gottlieb, Macromolecules 25 (1992) 4036.
[36] J. Pérez, J.Y. Cavalier, R.D. Calleja, J.L. Gomez Riballes, M.M. Pradas, A.R. Greus, Makromol. Chem. 192 (1991) 2141.
[37] J.M.G. Cowie, R. Ferguson, Polymer 34 (1993) 2135.
[38] A.J. Kovacs, J.J. Aklonis, J.M. Hutchinson, A.R. Ramos, J. Polym. Sci. B 17 (1979) 1097.
[39] J. Málek, S. Montserrat, Thermochim. Acta 313 (1998) 191.
[40] J.M. Hutchinson, M. Ruddy, J. Polym. Sci. B 26 (1988) 2341.
[41] A.P. Sokolov, Endeavour 21 (1997) 109.
[42] M. Schmidt, F.H.J. Maurer, J. Polym. Sci. B 36 (1998) 1061.
[43] W. Wunderlich, in: J. Brandrup, E. H. Immergut (Eds.), Polymer Handbook, 3rd ed., vol. V, Wiley, New York, 1989, p.77.
[44] A.J. Kovacs, Fort. Hoch-Polym. 3 (1963) 394.
[45] L.C.E. Struik, Polymer 38 (1997) 733.
[46] S.W. Shalaby, H.E. Bair, in: E.A. Turi (Ed.), Thermal Characterization of Polymeric Materials, Academic Press, New York, 1981, p. 413.
[47] V. Tangpasuthadol, A. Shefer, C. Yu, J. Zhou, J. Kohn, J. Appl. Polym. Sci. 63 (1997) 1441.
[48] I.M. Hodge, Macromolecules 16 (1983) 898.